Wiley
International Journal of Energy Research
Volume 2024, Article ID 1341603, 14 pages
https://doi.org/10.1155/2024/1341603

WILEY

Research Article

Numerical Investigation on the Indicated Mean Effective Pressure and Integral Heat Release Rate Variations under Different Key Operating Parameters of a Spark-Ignited Free Piston Engine Generator

Yong Liu,[1] Boru Jia,[2] Zixuan Yang,[2] Zhiyuan Zhang,[2] Chang Liu,[2] Wei Wang,[2] Huihua Feng,[2] Zhengxing Zuo,[2] and Tony Roskilly[3]

[1]*School of Energy and Power Engineering, North University of China, Taiyuan 030051, China*
[2]*School of Mechanical Engineering, Beijing Institute of Technology, Beijing 100081, China*
[3]*Department of Engineering, Durham University, Durham, DH1 3LE, UK*

Correspondence should be addressed to Zhiyuan Zhang; zhiyuan_zhang@bit.edu.cn

Received 8 October 2023; Revised 3 May 2024; Accepted 3 June 2024

Academic Editor: Hock Jin Quah

Free-piston engine generator is a new type of hybrid power device and is regarded as the next-generation energy conversion device which can replace the traditional internal combustion engine. This paper focused on the combustion stability and combines experimental results to study the key factors affecting the stability of the free-piston engine, such as ignition time, intake pressure, equivalence ratio, and operating frequency. The simulation results showed that as the ignition advance angle increased, the indicated mean effective pressure increased significantly and the coefficient of variation of the indicated mean effective pressure was effectively reduced from 15.55% to 1.02% as the advance in ignition time from −15 to −30°ECA. When the intake pressure was increased to 1.2 bar, the average value of indicated mean effective pressure reached about 5.15 bar. When the equivalence ratio was in the range of 1.0–1.4, the coefficient of variation of the indicated mean effective pressure can be kept below 10%. The indicated mean effective pressure decreased monotonically from 4.79 to 3.62 bar, and the coefficient of variation increased by five times as the engine speed increased as the engine speed increased from 1,000 to 2,500 RPM.

1. Introduction

1.1. Background. Emission levels, fossil fuel depletion, and increased prices of underground fuels are the main influential forces for researchers to find out an alternating way for emission reduction and making the engine independent from fossil and imported fuels [1, 2]. The ongoing depletion of oil resources and the growing environmental concerns arising from automobile emissions have made hybrid power an inevitable developmental trend [3, 4]. FPEG is directly coupled by the free-piston internal combustion engine and the linear motor and is regarded as the next generation energy conversion device which can replace the traditional internal combustion engine [5, 6]. Compared with conventional engines, FPEG eliminates the complex crank connecting rod mechanical, and the high-temperature and high-pressure gas in the combustion cylinder drives the motor to reciprocate in a straight line to generate electricity. The free-piston engine has the advantages of simple structure [7], variable compression ratio [8], high volumetric power density [9], low friction loss, and easy modular arrangement and has been a hot research topic in the field of internal combustion engines internationally.

1.2. Literature Review. Since the late 1990s, the University of West Virginia has been engaged in the design and development of a free-piston internal combustion power generation system. The first prototype utilized reflux scavenging and inlet injection and employed a dedicated starting coil to aid in ignition [10]. The cylinder diameter of the prototype free-piston internal combustion engine was 36.5 mm, and the maximum design stroke was 50 mm. The experimental results showed that the prototype involved completing a brief reciprocating

motion, with an average piston speed of 2.37 m/s, an operating frequency of 23.1 Hz, and a maximum power generation of 313 W [11, 12]. However, the system experienced frequent misfires. Atkinson et al. [13] established a complete working cycle simulation model, and the simulation results showed that the peak pressure in the cylinder increased with the decrease of the combustion duration, and the increase in the peak pressure in the cylinder led to an increase in the operating frequency, and the compression ratio of the system would increase at the same time. The operating frequency of the system depends on the quality of the moving parts, and the reduction in the mass of the moving parts results in a decrease in the operating frequency of the system [13]. Houdyschell [14] designed a two-stroke dual-cylinder dual-piston FPEG compression ignition prototype. And the prototype uses a high-pressure common rail for fuel supply, and fuel is injected directly into the cylinder through a direct injection injector. The results revealed that the homogeneous compression combustion mode increased the indication efficiency of the system, but the stability of the system was considerably sensitive to various parameters, rendering control difficulties [15].

Mikalsen et al. [16] proposed a piston motion control method based on the top dead center prediction, and the engine fuel injection quantity is based on the predicted piston top dead center position in the compression stroke rather than the actual measurement. The simulation results showed that the control method can reduce the time delay of the controller and accelerate the response speed of the system [17]. Jia et al. [18] established a MATLAB model which is validated by experimental data to simulate the starting and stable operation of a dual-cylinder type FPEG. The oscillating start strategy was successfully realized, and the source of interference was qualitatively analyzed based on the simplified dynamic model [19]. As evidenced through the in-depth research on the combustion and emission of FPEG, compared with traditional crank link engines, the stable operation of FPEG is more difficult and is easily affected by numerous critical factors such as intake, ignition, and operating frequency. The stability of FPEG operation is closely associated with the cyclic variation of the combustion process in the free-piston engine.

Since the 1970s, a large number of scholars have investigated the cyclic variation of spark engines, and the correlation between cyclic variation, engine emissions, and performance has been confirmed [20, 21]. Lyon [22] conducted an experimental study on a commercial four-cylinder engine, with the results confirming that the cycle variation could be eliminated and the economy of the engine could be increased by 6%. Wang and Ji [23] conducted an experimental study on the cyclic variation characteristics of a hydrogen-rich gasoline engine under different working conditions. The experimental results indicated that the coefficient of variation of the indicated mean effective pressure decreased obviously with the increase in hydrogen ratio [24]. At a fixed speed and inlet pressure, when the inlet hydrogen volume fraction increased from 0% to 4.5%, the relevant excess air ratio of the engine lean combustion limit increased from 1.45 to 2.55 [25]. Zhao et al. [26] evaluated the cyclic variation in the combustion process of a hydraulic free-piston engine (HFPE). The coefficient of variation and correlation coefficient were calculated, and the results showed that the cyclic variation of HFPE was primarily caused by the special motion law of the piston [26]. Such results provided a theoretical basis for controlling the cyclic variations of the system [27]. From the actual operation of the engine, cyclic changes in external conditions are almost inevitable. During the intake process, the pressurization and filtration of the air will affect the intake state [28, 29], resulting in changes in the initial gas conditions of each cycle, which in turn will lead to cycle changes in combustion.

Table 1: The specifications of the FPEG prototype.

Specifications	Values	Unit
Ignition method	Spark ignition	—
Engine displacement	130	cc
Design stroke	60	mm
Cylinder bore	52.5	mm
Compress ratio	8	—
Fuel type	Gasoline	—
Intake boosting	1.1	bar
Fuel delivery system	Port injection	—

Previous studies have indicated that an increase in cyclic variation can negatively impact vehicle comfort, as well as result in elevated exhaust emissions and reduced thermal efficiency. Thus, reducing cyclic fluctuations is of great significance to improving engine performance. Free-piston engine operates different from traditional engines, since the piston motion is not constrained by the crankshaft connecting rod. So, for free-piston engines, cyclic fluctuations are a bigger challenge. However, there are currently few studies on the influencing factors and change patterns of FPEG cycle variation.

1.3. Aims and Methodology. In this research, a complete dual-cylinder type FPEG system test bench was established, a three-dimensional FPEG model was constructed using the computational fluid dynamics (CFD) simulation software CONVERGE, and the model was calibrated through the experimental results. Firstly, the periodic variation of 50 consecutive cycles when the FPEG system works in dual-cylinder and single-cylinder mode is explored. The cyclic variation of the system under the single-cylinder operation mode and dual-cylinder working mode was investigated. Then, the effects of key parameters such as ignition time, intake pressure, equivalence ratio, and operating frequency on the cyclic variation of the combustion process of the FPEG system were investigated. This paper aims to provide a basis reference for the efficient and stable operation of the FPEG system.

2. FPEG Configuration and Experimental Setup

2.1. FPEG Configuration. The dual-cylinder type FPEG prototype which is designed by our present research group adopts a two-stroke reflux scavenging method for air exchange and uses gasoline fuel. The prototype design parameters and detailed specifications are shown in Table 1. The property of the fuel used in this study is showed in Table 2 [30, 31].

Table 2: The basic property of the fuel used in this study.

Property	Unit	Gasoline
Chemical formula	—	CnH1.87 n
Molecular weight	Kg kmal^{-1}	114.24
Equivalence ratio ignition lower limit in NTP air	—	0.7
Flammability limits in air at NTP	%vol.	1.4–7.6
Flammability limits (λ)	—	1.51–0.26
Flammability limits (ϕ)	—	0.66–3.85
Minimum ignition energy in air	mJ	0.28
Autoignition temperature at STP	°C	247–280
Mass lower heating value at STP	kJ/kg	44,500
Density of gas at STP	kg/m^3	750
Diffusivity in air	cm^2/s	~0.07
Octane number	—	87
Volumetric lower heating value at NTP	kJ/m^3	195,800
Stoichiometric air-to-fuel ratio	kg/kg	14.7
Volumetric fraction of fuel in air, $\lambda = 1$	—	0.0165
Laminar burning velocity	m/s	0.45
Laminar burning speed in NTP air	cm/s	37–43
Quenching distance in NTP air	cm	0.2
Flame temperature in air	K	2,470

NTP denotes normal temperature (293.15 K) and pressure (1 atm). STP denotes standard temperature (0°C) and pressure (1 bar).

During the stable generating process, the mover assembly which is composed of electric motor mover, pistons, and connecting rods moves from the top dead center of the left combustion chamber to the right side under the pressure of high-pressure gas. The permanent magnet fixed on the mover assembly passes through the inside of the coil, and the coil cuts the magnetic field line to generate induced electromotive force so as to output electric energy. The piston moves to the right and passes through the left exhaust port of the left cylinder. The left cylinder begins to scavenge until the piston moves to the left and passes through the left exhaust port again. At the same time, the fuel–air mixture in the right combustion chamber is compressed by the piston as it moves toward the top dead center of the opposite side. Upon reaching the predetermined ignition position, the mixture is ignited. The high-pressure gas propels the piston assembly toward the left until it reaches the top dead center of the opposite side, thereby completing a full working cycle.

2.2. Experimental Setup. The FPEG prototype working mode and working process is shown in Figure 1. According to the experimental requirements of the FPEG system, relevant sensors and analysis instruments were arranged in corresponding positions for accurate measurement. The technical parameters and measurement accuracy of the sensor are shown in Table 3 [32, 33].

The intake compression system used in the present study mainly included a screw air compressor (DHF-10PM), cast steel gas storage tank (1.58 MPa), freeze dryer (DHF-10), and air filter (DHF-QPS). The nominal volume flow rate of the air compressor was 0.54–1.35 m^3/min, and the rated pressure was 0.8 MPa, which was enough to meet the intake and pressurization requirements of the dual-cylinder FPEG system. The PMAC motion control system was adopted for the test control system of the FPEG prototype, and the control parameters are the injection position, ignition position, and motor force. The PXI Express data acquisition system of National Instruments was adopted for the test data acquisition module and was equipped with an NI PXIe-6356 data acquisition card, including eight analog input channels and two analog output channels. The sampling rate was 1.25 MS/s. The air–fuel ratio analyzer is HORIBA MEXA-730λ, which can achieve a measurement accuracy of $\pm$0.1 A/F. For power analysis, the YOKOGAWA DL950 power analyzer is used to monitor and analyze the voltage and current values of each phase in the three-phase circuit in real-time through the voltage difference probe and the current probe.

3. Modeling and Validation

3.1. Data Processing and Analysis. FPEG is not typically measured by crankshaft time. The time calculated by the zero-dimensional model is converted into equivalent crank angle (°*ECA*) to describe the piston displacement of the FPEG. The °*ECA* of the piston at the top dead center is defined as 0°*ECA*, and the conversion formula is as follows:

$$^{\circ}ECA = (t - t_0) \cdot f \cdot 360. \tag{1}$$

The calculation formula of indicated mean effective pressure (*IMEP*) is

$$IMEP = \frac{W_i}{V_s} = \frac{\oint pdV}{V_s}, \tag{2}$$

where W_i is the indicated work output per cylinder per operating cycle and V_s is the cylinder volume.

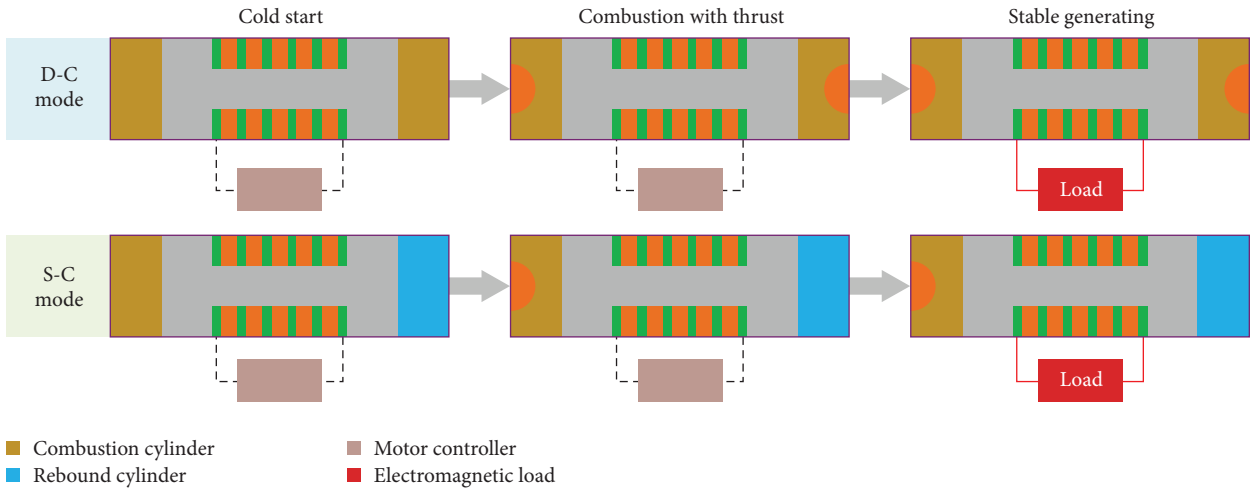

FIGURE 1: FPEG system working mode and working process (D-C mode, dual-cylinder working mode; S-C mode, single-cylinder working mode).

TABLE 3: FPEG system test bench sensors and measurement accuracy.

Instrument	Measured parameters	Range	Accuracy
Hall position sensor	Piston position	—	±25 μm
Air–fuel ratio analyzer	Air–fuel ratio	3.99–500.0	±9.1%A/F
Gas pressure sensor	Gas pressure	0–250 bar	±0.3%FS
Intake air flow sensor	Intake air flow	6–125 m^3/hr	±1.0%
Voltage sensor	Generation voltage	0–1,000 V	±1.0%
Current sensor	Generation current	0–300 A	±3.0%

The cylinder volume can be calculated by

$$V_L = \frac{\pi D^2}{4}(L + x), \tag{3}$$

$$V_R = \frac{\pi D^2}{4}(L - x), \tag{4}$$

where V_L is the left cylinder volume and V_R is the right cylinder volume. D is the cylinder diameter. L is half of the design stroke, and x is piston displacement.

The cyclic variation of the indicated mean effective pressure is a significant parameter that affects the stability and economy of engine operation [34]. The cyclic variation coefficient COV_{IMEP} of the indicated mean effective pressure of the engine was calculated so as to investigate the variation of the average indicated effective pressure of the free-piston engine the cyclic variation coefficient of the indicated mean effective pressure is defined as

$$COV_{IMEP} = \left[\sqrt{\sum_{k=1}^{N}\left(p_{IMEP,k} - \overline{p_{IMEP}}\right)^2/(N-1)\overline{p_{IMEP}}}\right] \times 100\%, \tag{5}$$

where COV is the coefficient of variation; $\overline{p_{IMEP}}$ is the mean value; and N is the total number of the sample data.

3.2. Multiphysics Coupling Simulation System. Figure 2 shows the multiphysics computing platform that combines simulation and experimentation of the FPEG system. Based on the dual-cylinder spark-ignited FPEG prototype developed by our research group, this paper establishes the FPEG multiphysics field coupling simulation experiment bench. The zero-dimensional computing model is coupled with the three-dimensional computing model. The coupling simulation system consists of a MATLAB model for calculating the dynamic characteristics of the piston motion and a three-dimensional CFD simulation model for calculating the working process in combustion cylinder. The piston displacement calculated by the kinematic model is used as the input of the CFD model. The FPEG prototype provides boundary conditions and engine parameters for the simulation model.

In order to study cycle to cycle variation of the free-piston engine, 10 stable and continuous cycles were selected from the calculation results of the CFD simulation model. The parameter settings of the initial conditions and boundary conditions in the calculation process are based on the experimental results of the physical prototype, and several parameters are set according to the empirical values. The specific boundary condition parameters are shown in Table 4. The reaction mechanism selected by the model is shown in Table 5.

3.3. Model Validation. The results of the experiment and simulation were compared, so as to verify the effectiveness of the established simulation model. Figure 3 shows the

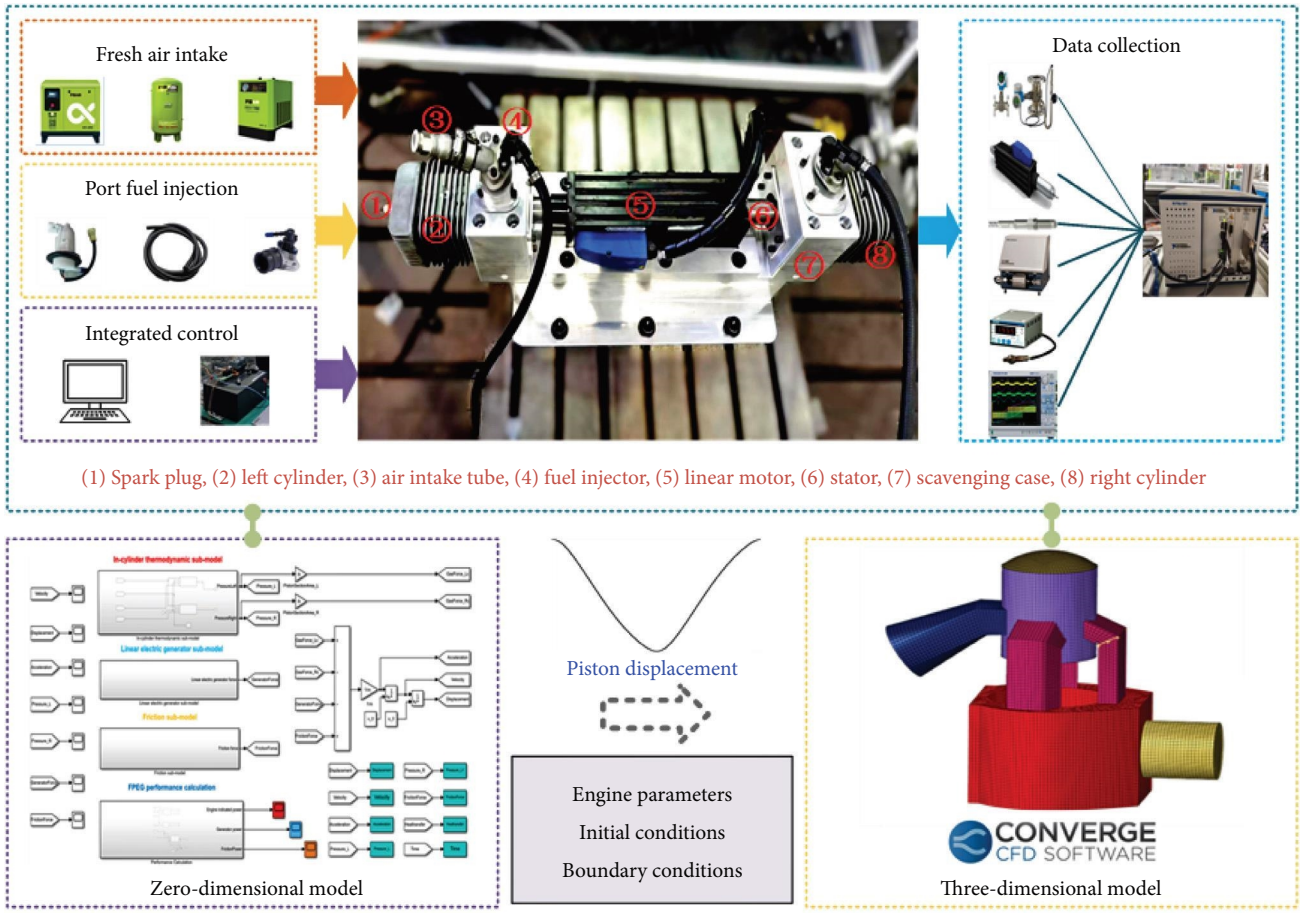

Figure 2: FPEG multiphysics coupling simulation experimental platform.

Table 4: The boundary condition parameters of the CFD model.

Parameter	Values	Unit
Intake pressure	1.1	bar
Intake temperature	300	K
Exhaust pressure	1	bar
Exhaust temperature	500	K
Cylinder head temperature	550	K
Piston face temperature	550	K
Cylinder wall temperature	450	K

Table 5: Selection of reaction mechanism of the CFD model.

Description	Model
Turbulent flow model	k-zeta-f model
Combustion model	ECFM model
Heat transfer model	Han–Reitz model
NOx formation mechanism	Extension Zeldovitch model
Ignition model	Spherical selection module

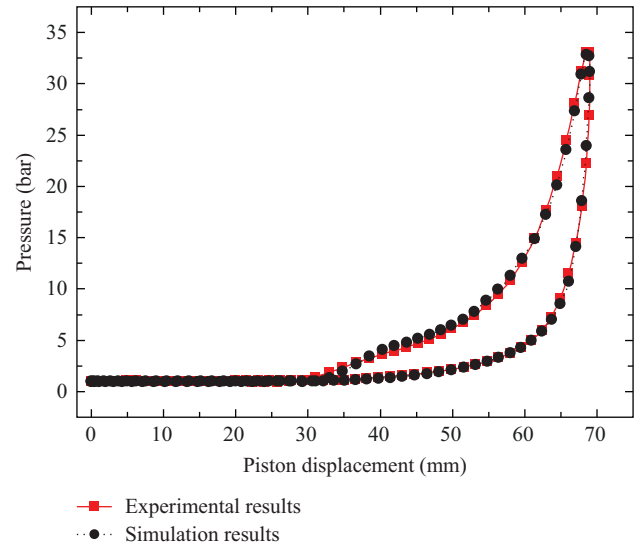

Figure 3: In-cylinder gas pressure changes: experimental and simulation results.

comparison of the simulation data and experimental data under the same boundary conditions and operating conditions. An observation can be made that in the compression stroke and high-pressure stage, the simulation data and experimental data are basically consistent. The maximum cylinder pressure of the simulation is 33.69 bar, the maximum cylinder pressure of the experiment is 33.46 bar, and the error is about 0.7%. The maximum error value is within

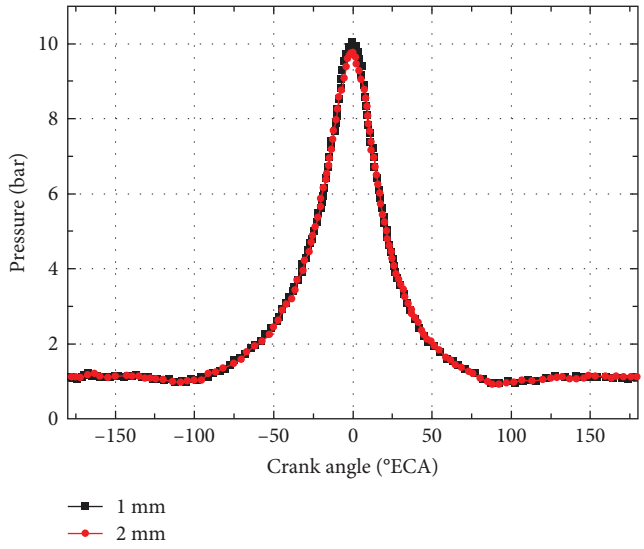

FIGURE 4: Comparison of in-cylinder pressure with different mesh sizes.

5%, indicating that the accuracy of the established model met the research requirements.

3.4. Grid Independence Verification. In order to verify the numerical simulation model, the sensitivity of the proposed numerical simulation model to different mesh sizes has been analyzed by our previous research [35]. Under the condition of non-combustion, $1 \times 1 \times 1$ mm and $2 \times 2 \times 2$ mm grids were applied to simulate the in-cylinder working process of the dual-cylinder free-piston linear motor. The simulation results are demonstrated in Figure 4. It can be clearly seen that there are few differences in the in-cylinder pressure curve among the grids with the size of $1 \times 1 \times 1$ mm and $2 \times 2 \times 2$ mm. In order to ensure the stability and accuracy of numerical calculations, a fully orthogonal hexahedral grid with a basic size of 2 mm is used for global calculations. Taking into account the dramatic changes in temperature gradient, velocity gradient, and pressure gradient in the local area, the size ratio of adjacent grids is less than $2 \times 2 \times 2$ mm.

4. Results and Discussion

4.1. Experimental Data and Analysis. Figure 5 shows continuous 50-cycle piston displacement and in-cylinder pressure changes collected from experimental prototype. However, from the current experimental results, there is still a large space for improvement in FPEG performance. As can be seen from Figure 5, the peak pressure of the engine in the single-cylinder working mode is higher, and the fluctuation is smaller than that in the dual-cylinder working mode. Compared with the dual-cylinder working mode, the free-piston cylinder in the single-cylinder working mode has more sufficient ventilation time.

The periodic variation of 50 consecutive cycles when the FPEG system works in dual-cylinder and single-cylinder mode is explored. Based on the results shown in Figure 6, it can be inferred that the single-cylinder working mode of the free-piston engine generator is more stable than the dual-cylinder working mode. The 10.11% COV_{IMEP} value for the dual-cylinder working mode is much greater compared to the 0.83% COV_{IMEP} value for the single-cylinder working mode.

4.2. Cyclic Variation under Different Ignition Time of the Simulation Results. Ignition timing is the concept of ignition advance angle in traditional internal combustion engines. This ignites the combustible mixture in the combustion chamber. From the ignition moment until the piston reaches the compression top dead center, the angle the crankshaft rotates during this period is called the ignition advance angle. For example, if the ignition occurs 15°*ECA* before the top dead center, we call the ignition time of this cycle −15°*ECA*.

Figure 7(a) shows the *IMEP* changes with the number of cycles. It can be seen from the simulation results that the *IMEP* increased significantly with the increase in ignition advance angle. With the advance in ignition time from −15 to −30°*ECA*, the *IMEP* increased from 3.29 to 5.56 bar, an increase of 69%. With the advance in ignition time, the mixture burned rapidly, and the combustion duration was significantly shortened, as shown in Figure 8.

Figure 7(b) shows the COV_{IMEP} changes under different ignition times. The results indicated that an earlier ignition time had a notable positive impact on the COV_{IMEP} of the free-piston engine, which was primarily due to the fact that in the early stage of combustion, although the fire core is still small, it can be removed from the spark plug area by large-scale flow in the cylinder. This phenomenon occurred in a random manner and had a significant impact on the subsequent propagation of combustion, resulting in cyclic changes. For FPEG, early ignition promoted the rapid and complete combustion of the fuel–air mixture, and the combustion duration was significantly shortened.

Figure 8 shows the relationship between the integral heat release rate and the equivalent crank angle under different ignition time. The integral heat release rate is defined as the percentage of the integral heat release of a certain crank angle to the total heat release of the whole combustion process. Additionally, the flame propagation (CA10-90) period is also based on the integral heat release, which is defined as the crank angle duration from 10% to 90% of the total fuel heat release from the spark plug ignition. As shown in Figure 8, CA10-90 was shortened after early ignition because more fuel was burned around the top dead center as the ignition time advanced. When the ignition was advanced, COV_{IMEP} was effectively reduced from 15.55% at −15°*ECA* to 1.02% at −30°*ECA*. Shortening the combustion duration is beneficial for reducing the cyclic variation of the free-piston engine.

Figure 9 shows the changes of in-cylinder gas peak pressure (P_{max}) and its cyclic variation coefficient (COV_{Pmax}) at 2,000 RPM and different ignition times. Under the same conditions, COV_{Pmax} increased first and then decreased with the delay in ignition time.

When the ignition time is delayed, owing to the decrease in combustion temperature and pressure, the combustion duration of the mixture in the cylinder would inevitably be

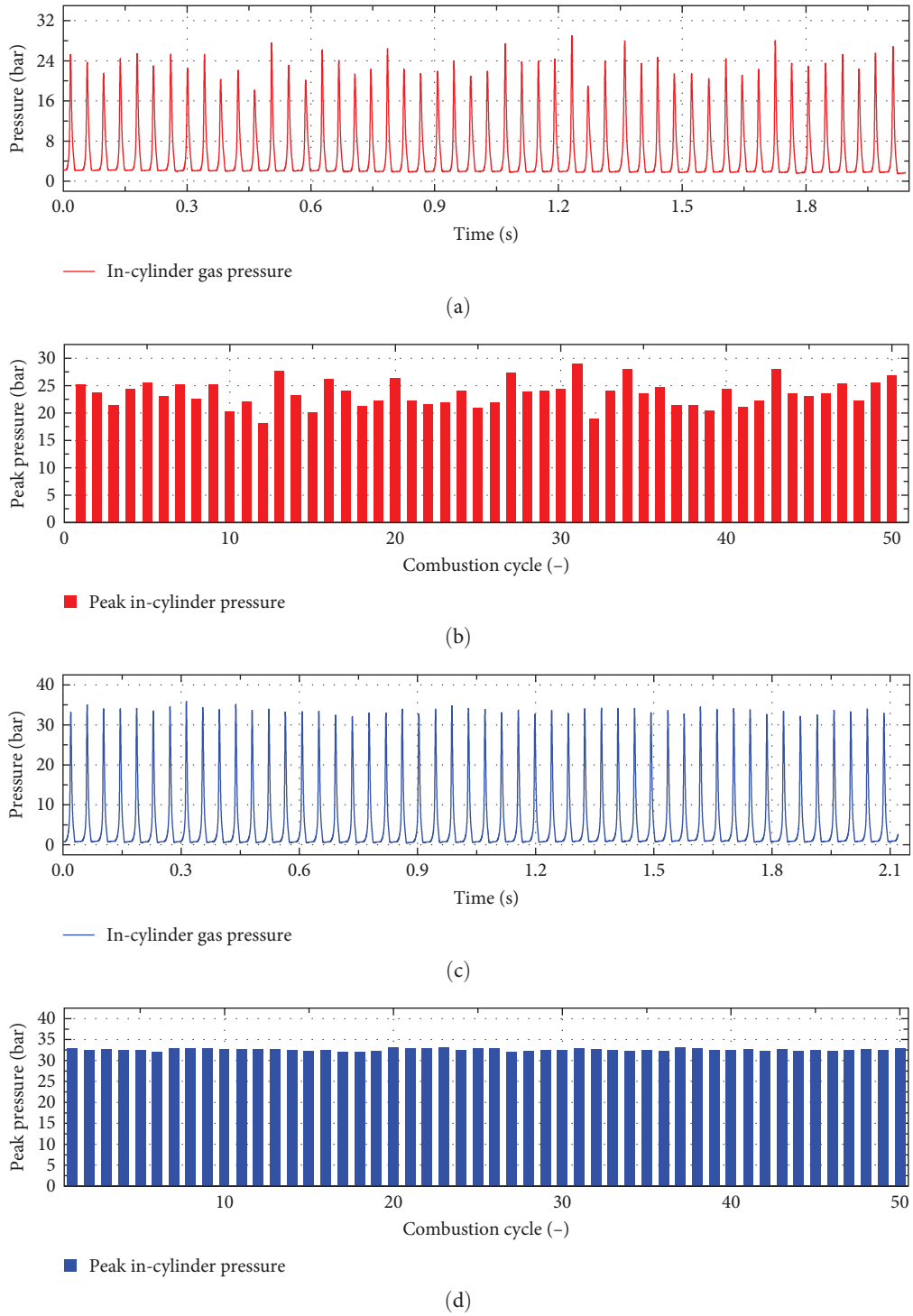

FIGURE 5: Continuous 50-cycle piston displacement and in-cylinder pressure changes. (a) In-cylinder gas pressure in the dual-cylinder working mode. (b) Peak in-cylinder gas pressure in the dual-cylinder working mode. (c) In-cylinder gas pressure in the single-cylinder working mode. (d) Peak in-cylinder gas pressure in the single-cylinder working mode.

prolonged. Therefore, COV_{IMEP} increased significantly with the delay in excessive ignition time. In contrast, peak cylinder pressure is affected by both combustion and piston motion. An observation can be made from Figure 9(a) that in the case of ignition delay, the influence of piston motion on peak cylinder pressure became increasingly obvious with the further extension of combustion time. Because the pressure rise caused by piston motion was more stable than that caused by combustion at a constant engine speed, COV_{Pmax} decreased again when the ignition was delayed.

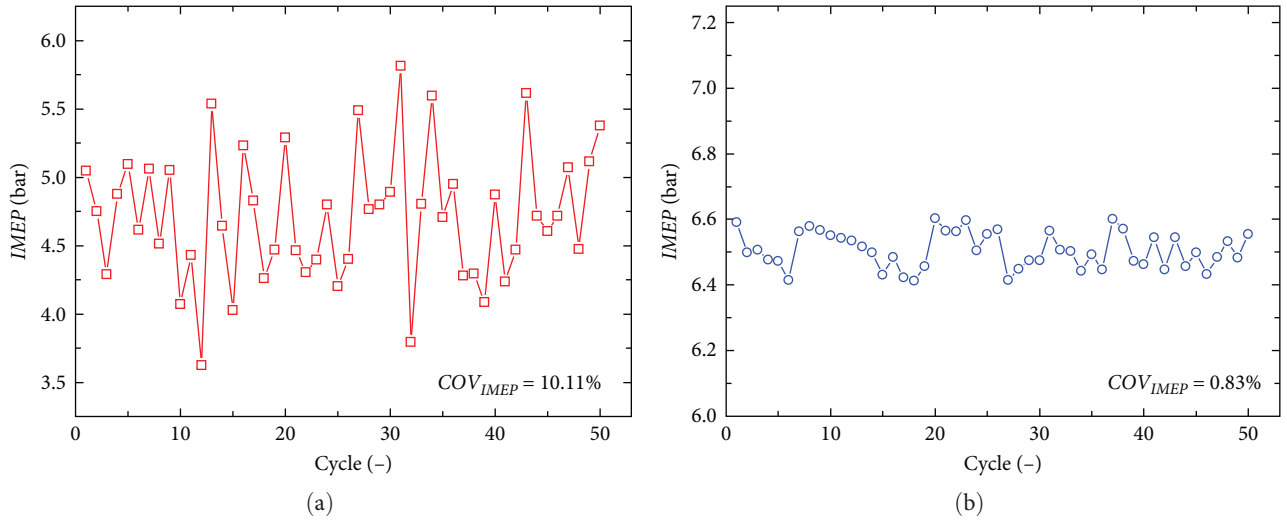

FIGURE 6: Indicated mean effective pressure of 50 cycles of the FPEG system. (a) In the dual-cylinder working mode. (b) In the single-cylinder working mode.

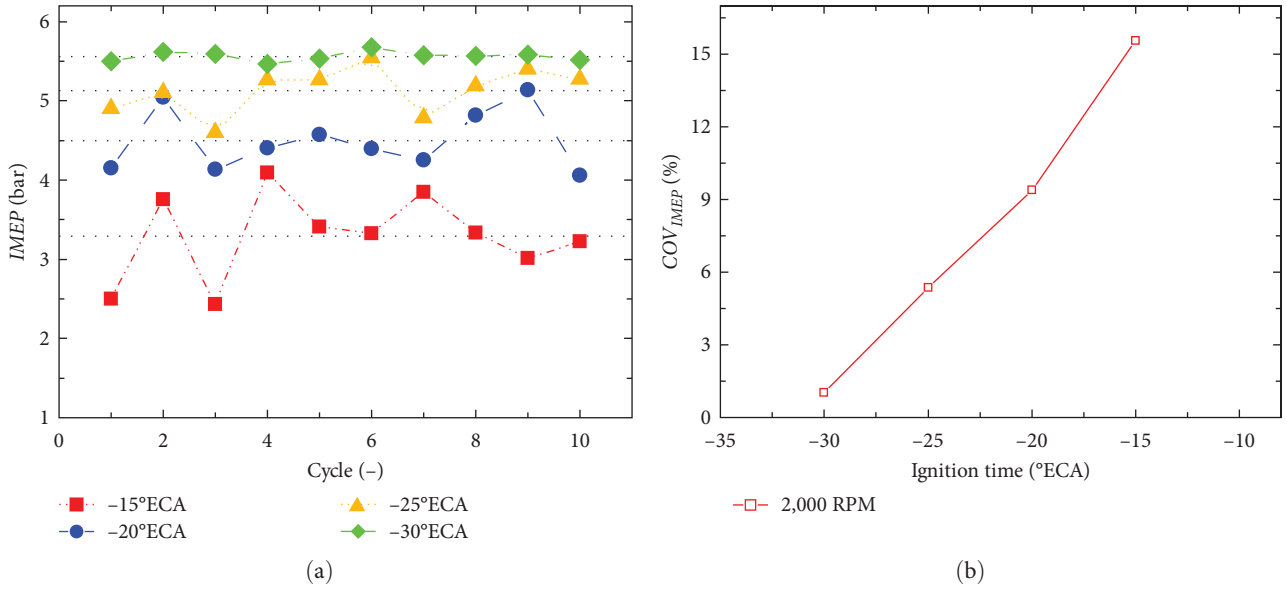

FIGURE 7: The evolution of *IMEP* and $COVp_i$ at the different ignition timings. (a) *IMEP* and (b) COV_{IMEP}.

4.3. Cyclic Variation under Different Intake Pressures of the Simulation Results. Figure 10 shows the evolution of the indicated mean effective pressure with the number of cycles under different intake pressures at the same ignition time and engine speed. The *IMEP* increased with the increase in intake pressure. When the intake pressure increases from 1.05 to 1.20 bar, the average value of *IMEP* reached to 5.15 bar. When the intake pressure increased, the quality of the fuel entering the cylinder increased, the flow of the working fluid in the cylinder is enhanced, and the turbulent kinetic energy increased, as shown in Figure 10. When the intake pressure increased from 1.05 to 1.20 bar, the peak value of turbulent kinetic energy increased from 28.1 to 244.7 m^2/s^2. The increase of turbulent kinetic energy led to the acceleration of fuel evaporation rate and the more uniform mixing of the mixture. In addition, it can be seen from Figure 10(b) that under different intake pressures, COV_{IMEP} did not change much and remained between a small value. It indicates that FPEG could operate stably and continuously under different intake pressures.

Scavenging efficiency refers to the mass of fresh air charge left in the cylinder before combustion divided by the sum of the mass of fresh air charge left in the cylinder before combustion, and the mass of residual gas left in the cylinder after the exhaust port is closed in the previous working cycle:

$$\eta = \frac{m_1}{m_0} = \frac{m_1}{m_1 + m_r}, \tag{6}$$

where η is scavenging efficiency, m_1 is the mass of fresh air charge left in the cylinder before combustion, m_0 is the sum of the mass of fresh air charge left in the cylinder before

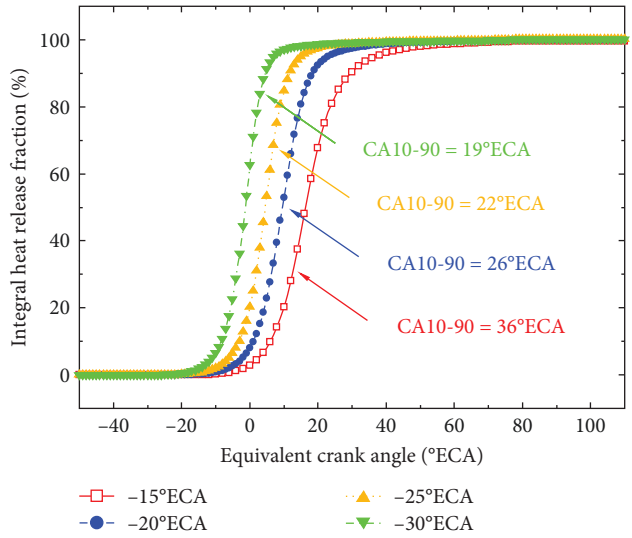

FIGURE 8: Integral heat release fraction at the different ignition timings.

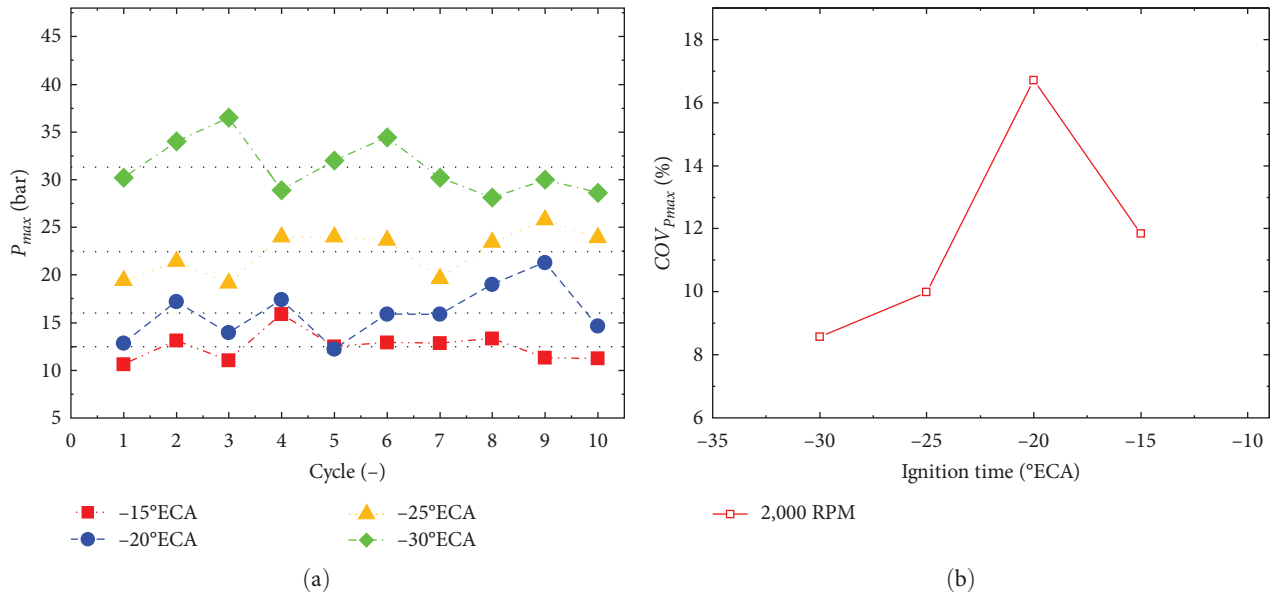

FIGURE 9: The evolution of P_{max} and COV_{Pmax} under different ignition times. (a) P_{max} and (b) COV_{Pmax}.

combustion and the mass of residual gas left in the cylinder after the exhaust port is closed in the previous working cycle, and m_r is the mass of residual gas left in the cylinder after the exhaust port is closed in the previous working cycle.

In contrast, the cyclic variation of FPEG is more obviously affected by the ignition time. Cyclic variation is mainly caused by the difference in ignition and combustion process in each cycle. The most significant influencing factors are mixture composition fluctuation and gas motion state fluctuation. Figure 11 shows the scavenging efficiency of FPEG under different intake pressures and frequencies. Evidently, except for some extreme cases, the scavenging efficiency of FPEG was maintained at a good state, and the composition of the mixture in the cylinder had little fluctuation. At the same time, the ignition time and ignition energy did not change, which ensured that the cyclic variation of FPEG under different inlet pressures was not large.

4.4. Cyclic Variation under Different Equivalence Ratios of the Simulation Results. The equivalence ratio, also known as "fuel coefficient" or "remaining oil coefficient," is the ratio of the theoretical amount of air required for complete combustion to the actual amount of air supplied when fuel is burned.

Figure 12 shows the *IMEP* and COV_{IMEP} change under different equivalence ratios. It can be seen from the simulation results that the equivalence ratio has a great influence on both *IMEP* and COV_{IMEP}. When the equivalence ratio is 1.2, the average value of *IMEP* is the largest.

From Figure 13, it can be observed that when the equivalence ratio decreased from 1.2 to 0.8, the combustion heat

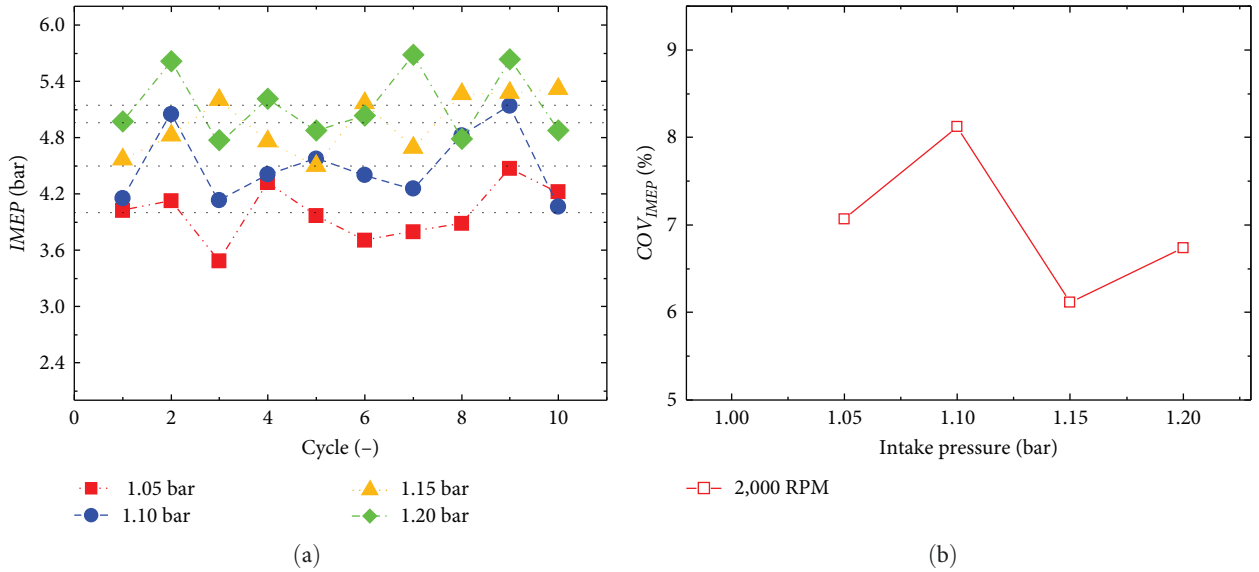

Figure 10: The evolution of *IMEP* and COV_{IMEP} under different intake pressures. (a) *IMEP* and (b) COV_{IMEP}.

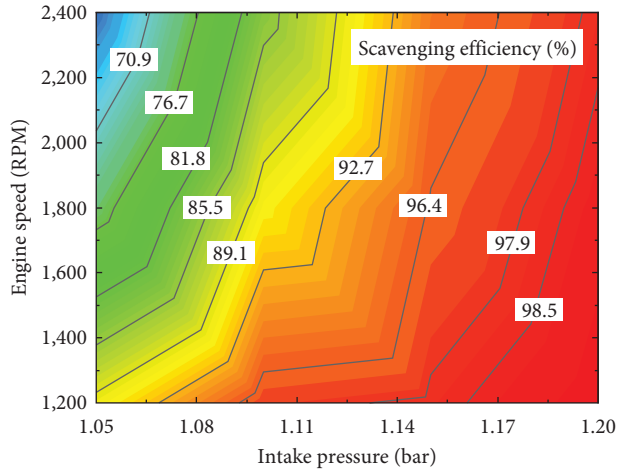

Figure 11: Scavenging efficiency of FPEG under different intake pressures and frequencies.

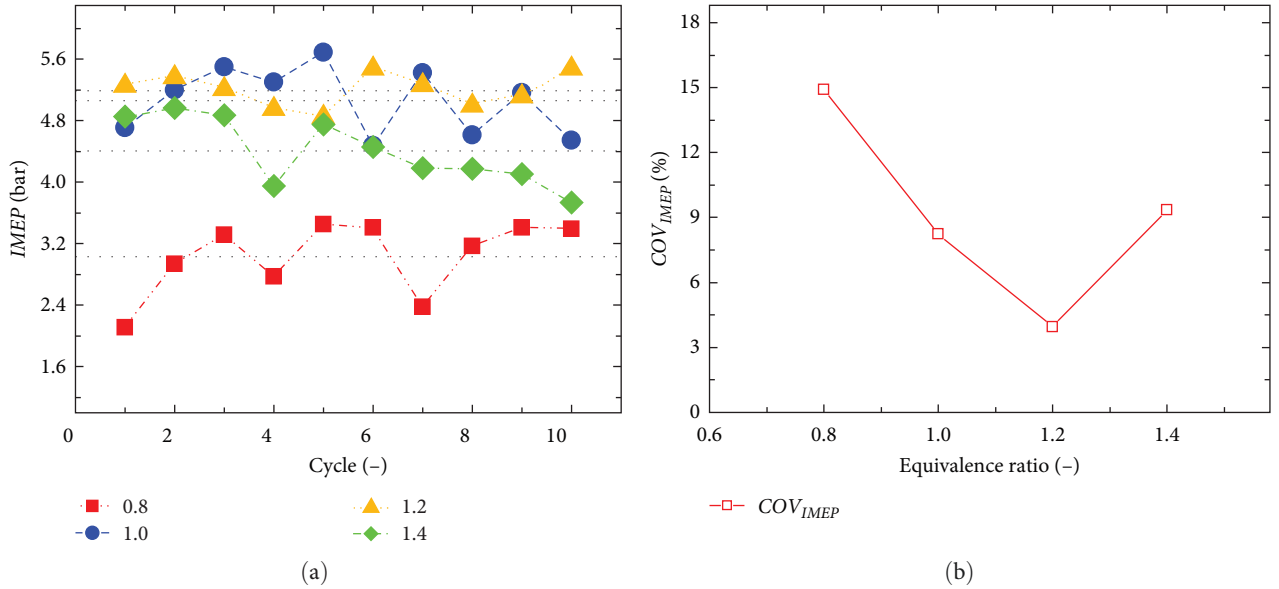

Figure 12: The evolution of *IMEP* and COV_{pi} at different equivalence ratios. (a) *IMEP* and (b) COV_{IMEP}.

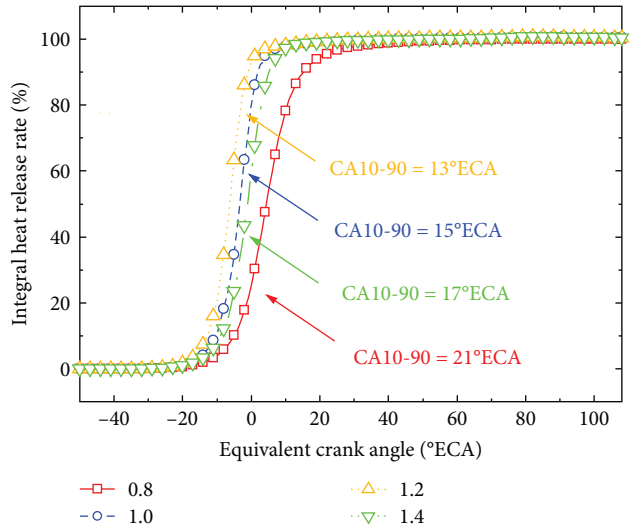

FIGURE 13: Integral heat release fraction at different equivalence ratios.

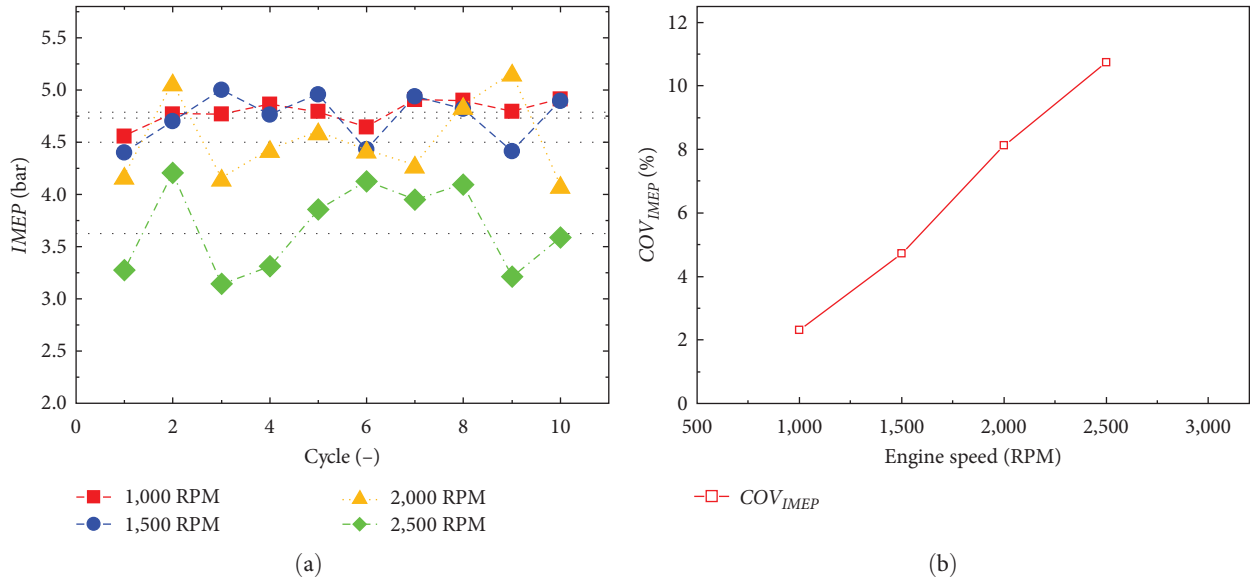

FIGURE 14: The evolution of *IMEP* and COV_{IMEP} under different engine speeds. (a) *IMEP* and (b) COV_{IMEP}.

release process is significantly prolonged, resulting in the whole combustion process deviating from the top dead center. During this process, the combustion duration is extended by 8°*ECA*. The free-piston engine released a large amount of heat in a short time, which promoted the continuous increase of in-cylinder pressure.

Another noteworthy trend is that the COV_{IMEP} can be kept below 10% when the equivalence ratio is around 1.0. However, as the concentration of the mixture further dilutes, the COV_{IMEP} of the engine increased sharply. When the equivalence ratio dropped to 0.8, COV_{IMEP} increased significantly to 14.9%, which means that under lean combustion conditions, the probability of partial combustion or even misfire of the engine will be greatly increased. For the FPEG, any factor that slows down the combustion process will increase its cyclic variation. Therefore, in order to better run the stability, the equivalence ratio should be selected in a relatively dense range (1.0–1.2).

4.5. Cyclic Variation under Different Engine Speeds of the Simulation Results. Figure 14 shows the *IMEP* and COV_{IMEP} change under different engine speed. The *IMEP* decreased from 4.79 to 3.62 bar as the engine speed increased from 1,000 to 2,500 RPM. This reduction is mainly due to the engine scavenging efficiency decreased when the engine speed increases (Figure 15), and the residual gas in the cylinder increased. The residual gas coefficient caused the combustion rate to decrease, as shown in Figure 16.

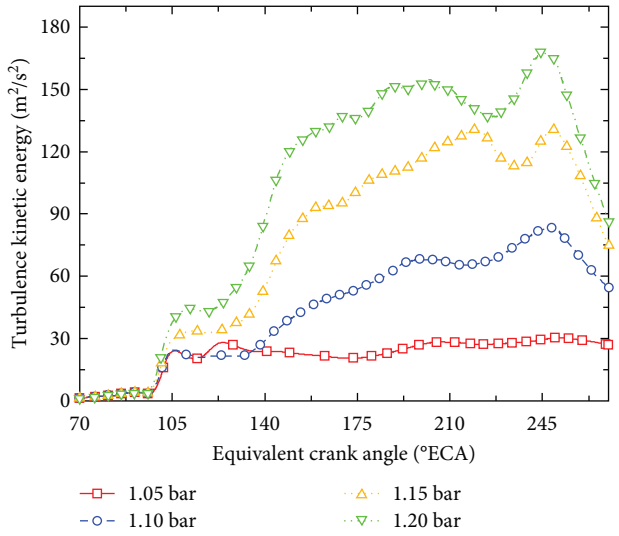

FIGURE 15: In-cylinder turbulent kinetic energy change.

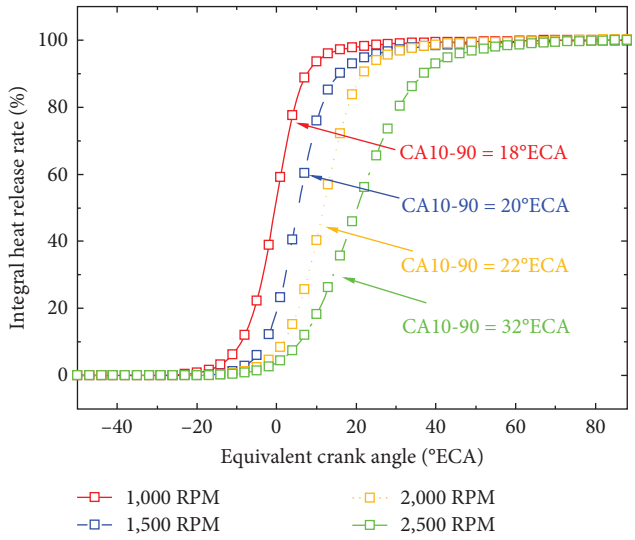

FIGURE 16: Integral heat release fraction under different engine speeds.

The COV_{IMEP} of FPEG under different speeds is depicted in Figure 14(b). The coefficient of variation increases as the engine speed increases, with the COV_{IMEP} reaching 2.3% and exceeding 10% at 2,500 RPM. It can be seen from Figure 14 that when the ignition timing is fixed, the heat release process is significantly extended with the increase in speed, leading to the deviation of the whole combustion process from top dead center. When the speed increased from 1,000 to 2,500 RPM, the rapid combustion duration is prolonged by 14°*ECA*. More heat release processes occurred on the power stroke, resulting in the reduction of combustion efficiency, which also explains the decrease in *IMEP*.

5. Conclusion

In this paper, a complete dual-cylinder type FPEG system test bench was established, a three-dimensional model was constructed using the CFD simulation software CONVERGE, and the model was calibrated through the experimental results. The effects of key parameters such as ignition time, intake pressure, equivalence ratio, and operating frequency on the cyclic variation of the combustion process of the FPEG system were investigated. The following results were obtained.

(1) The single-cylinder working mode of the free-piston engine generator is more stable than the dual-cylinder working mode. The 10.11% COV_{IMEP} value for the dual-cylinder working mode is much greater compared to the 0.83% COV_{IMEP} value for the single-cylinder working mode.

(2) With the increase in ignition advance time, the average *IMEP* value increased significantly. When the advance in ignition time increases from −15 to −30°*ECA*, the average *IMEP* increased from 3.29 to 5.56 bar, an increase of 69%. With the advance in ignition, the COV_{IMEP} is effectively reduced, and the COV_{IMEP} value decreased from 15.55% at −15°*ECA* to 1.02% at −30°*ECA*.

(3) When the intake pressure increases from 1.05 to 1.2 bar, the average value of *IMEP* reached about 5.15 bar, and the peak value of turbulent kinetic energy increased from 28.1 to 244.7 m^2/s^2. The increase of turbulent kinetic energy led to the acceleration of fuel evaporation rate and the more uniform mixing of the mixture.

(4) When the equivalence ratio is 1.2, the average value of *IMEP* is the largest. At this time, the combustion speed in the cylinder is fastest. When the equivalence ratio is greater than 0.8, COV_{IMEP} can be kept below 10%, which means that FPEG can operate stably. As the concentration of the mixture further dilutes, the COV_{IMEP} of the engine increased sharply. To achieve better operational stability, the equivalence ratio should be selected in a relatively dense range (1.0–1.2).

(5) As the engine speed increased, the average value of *IMEP* decreased monotonically from 4.79 to 3.62 bar, a decrease of about 25%. When the speed increased from 1,000 to 2,500 RPM, the rapid combustion duration is prolonged by 14°*ECA*. Such results indicate that the engine operation became more unstable at higher speeds.

Nomenclature

°ECA:	Equivalent crankshaft angle
CA:	Crankshaft angle
CFD:	Computational fluid dynamics
COV:	Coefficient of variation
D-C mode:	Dual-cylinder working mode
FPEG:	Free-piston engine generator
HFPE:	Hydraulic free-piston engine
IMEP:	Indicated mean effective pressure
NTP:	Normal temperature (293.15 K) and pressure (1 atm)

S-C mode: Single-cylinder working mode
STP: Standard temperature (0°C) and pressure (1 bar).

Data Availability

Data will be made available on request.

Conflicts of Interest

The authors declare that they have no conflicts of interest.

Acknowledgments

This work is funded by the Chinese Government, and we thank the financial sponsors.

References

[1] S. Lalsangi, V. S. Yaliwal, N. R. Banapurmath et al., "Influence of hydrogen injection timing and duration on the combustion and emission characteristics of a diesel engine operating on dual fuel mode using biodiesel of dairy scum oil and producer gas," *International Journal of Hydrogen Energy*, vol. 48, no. 55, pp. 21313–21330, 2023.

[2] D. Barik, B. J. Bora, P. Sharma et al., "Exploration of the dual fuel combustion mode on a direct injection diesel engine powered with hydrogen as gaseous fuel in port injection and diesel-diethyl ether blend as liquid fuel," *International Journal of Hydrogen Energy*, vol. 52, pp. 827–840, 2024.

[3] W. Gu, X. Zhao, X. Yan, C. Wang, and Q. Li, "Energy technological progress, energy consumption, and CO2 emissions: empirical evidence from China," *Journal of Cleaner Production*, vol. 236, Article ID 117666, 2019.

[4] S. Singh, D. G. Rao, and M. Dixit, "Experimental investigation of a reactivity controlled compression ignition engine fuelled with liquified petroleum gas," *Universal Journal of Mechanical Engineering*, vol. 11, no. 2, pp. 25–35, 2023.

[5] R. Mikalsen and A. P. Roskilly, "A review of free-piston engine history and applications," *Applied Thermal Engineering*, vol. 27, no. 14-15, pp. 2339–2352, 2007.

[6] N. B. Hung and O. Lim, "A review of free-piston linear engines," *Applied Energy*, vol. 178, pp. 78–97, 2016.

[7] B. Jia, Z. Zuo, G. Tian, H. Feng, and A. P. Roskilly, "Development and validation of a free-piston engine generator numerical model," *Energy Conversion and Management*, vol. 91, pp. 333–341, 2015.

[8] Z. Zhang, H. Feng, B. Jia, Z. Zuo, A. Smallbone, and A. P. Roskilly, "Effect of the stroke-to-bore ratio on the performance of a dual-piston free piston engine generator," *Applied Thermal Engineering*, vol. 185, Article ID 116456, 2021.

[9] C. Li, Y. Wang, B. Jia, and A. P. Roskilly, "Application of Miller cycle with turbocharger and ethanol to reduce NOx and particulates emissions from diesel engine—a numerical approach with model validations," *Applied Thermal Engineering*, vol. 150, pp. 904–911, 2019.

[10] N. Clark, S. Nandkumar, C. Atkinson, and R. Atkinson, "Operation of a smallbore two-stroke linear engine," in *Proceeding of the Fall Technical Conference of the ASME Internal Combustion Engine Division*, vol. 31, pp. 33–40, 1998.

[11] P. Famouri, W. R. Cawthorne, N. Clark et al., "Design and testing of a novel linear alternator and engine system for remote electrical power generation," *IEEE Power Engineering Society*, vol. 1, pp. 108–112, 1999.

[12] M. C. Robinson and N. N. Clark, "Fundamental explorations of spring-varied, free piston linear engine devices," *Journal of Engineering for Gas Turbines and Power*, vol. 137, no. 10, Article ID 101502, 2015.

[13] C. M. Atkinson, S. Petreanu, N. N. Clark et al., "Numerical simulation of a two-stroke linear engine-alternator combination," *SAE Transactions*, pp. 1416–1430, 1999.

[14] D. Houdyschell, *A Diesel Two-Stroke Linear Engine*, West Virginia University, 2000.

[15] S. Petreanu, *Conceptual Analysis of a Four-Stroke Linear Engine*, West Virginia University, 2001.

[16] R. Mikalsen, E. Jones, and A. P. Roskilly, "Predictive piston motion control in a free-piston internal combustion engine," *Applied Energy*, vol. 87, no. 5, pp. 1722–1728, 2010.

[17] B. Jia, R. Mikalsen, A. Smallbone, Z. Zuo, H. Feng, and A. P. Roskilly, "Piston motion control of a free-piston engine generator: a new approach using cascade control," *Applied Energy*, vol. 179, pp. 1166–1175, 2016.

[18] B. Jia, G. Tian, H. Feng, Z. Zuo, and A. P. Roskilly, "An experimental investigation into the starting process of free-piston engine generator," *Applied Energy*, vol. 157, pp. 798–804, 2015.

[19] B. Jia, A. Smallbone, R. Mikalsen, H. Feng, Z. Zuo, and A. P. Roskilly, "Disturbance analysis of a free-piston engine generator using a validated fast-response numerical model," *Applied Energy*, vol. 185, pp. 440–451, 2017.

[20] R. K. Barton, S. S. Lestz, and W. E. Meyer, "An empirical model for correlating cycle-by-cycle cylinder gas motion and combustion variations of a spark ignition engine," *SAE Transactions*, pp. 695–707, 1971.

[21] M. Rashidi, "The nature of cycle-by-cycle variation in the S.I. engine from high speed photographs," *Combustion and Flame*, vol. 42, pp. 111–122, 1981.

[22] D. Lyon, "Knock and cyclic dispersion in a spark ignition engine," in *International Conference on Petroleum Based Fuels and Automotive Applications*, pp. 105–115, Transport Research Laboratory, 1986.

[23] S. Wang and C. Ji, "Cyclic variation in a hydrogen-enriched spark-ignition gasoline engine under various operating conditions," *International Journal of Hydrogen Energy*, vol. 37, no. 1, pp. 1112–1119, 2012.

[24] H. Wang, C. Ji, C. Shi, Y. Ge, S. Wang, and J. Yang, "Development of cyclic variation prediction model of the gasoline and n-butanol rotary engines with hydrogen enrichment," *Fuel*, vol. 299, Article ID 120891, 2021.

[25] T. Su, C. Ji, S. Wang, L. Shi, J. Yang, and X. Cong, "Reducing cyclic variation of a gasoline rotary engine by hydrogen addition under various operating conditions," *International Journal of Hydrogen Energy*, vol. 42, no. 40, pp. 25428–25435, 2017.

[26] Z. Zhao, D. Wu, Z. Zhang, F. Zhang, and C. Zhao, "Experimental investigation of the cycle-to-cycle variations in combustion process of a hydraulic free-piston engine," *Energy*, vol. 78, pp. 257–265, 2014.

[27] Z. Zhao, F. Zhang, Y. Huang, C. Zhao, and F. Guo, "An experimental study of the hydraulic free piston engine," *Applied Energy*, vol. 99, pp. 226–233, 2012.

[28] T. Dziubak and M. Karczewski, "Experimental study of the effect of air filter pressure drop on internal combustion engine performance," *Energies*, vol. 15, no. 9, Article ID 3285, 2022.

[29] T. Dziubak, "Experimental studies of powercore filters and pleated filter baffles," *Materials*, vol. 15, no. 20, Article ID 7292, 2022.
[30] R. K. Mehra, H. Duan, R. Juknelevičius, F. Ma, and J. Li, "Progress in hydrogen enriched compressed natural gas (HCNG) internal combustion engines—a comprehensive review," *Renewable and Sustainable Energy Reviews*, vol. 80, pp. 1458–1498, 2017.
[31] A. K. Thakur, A. K. Kaviti, R. Mehra, and K. K. S. Mer, "Progress in performance analysis of ethanol-gasoline blends on SI engine," *Renewable and Sustainable Energy Reviews*, vol. 69, pp. 324–340, 2017.
[32] Z. Yang, Z. Zhang, C. Liu et al., "Effect of ignition timing on the combustion process of a port injection free piston linear generator: a system level multi-physics coupling method," *Fuel*, vol. 333, Article ID 126520, 2023.
[33] Z. Zhang, H. Feng, H. He et al., "Demonstration of a single/dual cylinder free-piston engine generator prototype: milestone achieved on system stability," *Energy*, vol. 278, Article ID 127948, 2023.
[34] D. Goryntsev, A. Sadiki, M. Klein, and J. Janicka, "Large eddy simulation based analysis of the effects of cycle-to-cycle variations on air–fuel mixing in realistic DISI IC-engines," *Proceedings of the Combustion Institute*, vol. 32, no. 2, pp. 2759–2766, 2009.
[35] X. Yan, H. Feng, Z. Zuo, B. Jia, Z. Zhang, and W. Wang, "Research on the combustion and emission characteristics of homogeneous dual cylinder free piston generator by ignition strategy," *Journal of Cleaner Production*, vol. 328, Article ID 129564, 2021.